Biophysical Journal
Article

Biophysical Society

Unfolding of CPR3 Gets Initiated at the Active Site and Proceeds via Two Intermediates

Vaibhav Kumar Shukla,[1] Jai Shankar Singh,[2] Neha Vispute,[1] Basir Ahmad,[1] Ashutosh Kumar,[2,*] and Ramakrishna V. Hosur[1,3,*]

[1]UM-DAE-Centre for Excellence in Basic Sciences, University of Mumbai, Kalina Campus, Mumbai, India; [2]Department of Biosciences and Bioengineering, Indian Institute of Technology, Mumbai, India; and [3]Department of Chemical Sciences, Tata Institute of Fundamental Research, Mumbai, India

ABSTRACT Cyclophilin catalyzes the ubiquitous process "peptidyl-prolyl *cis-trans* isomerization," which plays a key role in protein folding, regulation, and function. Here, we present a detailed characterization of the unfolding of yeast mitochondrial cyclophilin (CPR3) induced by urea. It is seen that CPR3 unfolding is reversible and proceeds via two intermediates, I1 and I2. The I1 state has native-like secondary structure and shows strong anilino-8-naphthalenesulphonate binding due to increased exposure of the solvent-accessible cluster of non-polar groups. Thus, it has some features of a molten globule. The I2 state is more unfolded, but it retains some residual secondary structure, and shows weak anilino-8-naphthalenesulphonate binding. Chemical shift perturbation analysis by ^{1}H-^{15}N heteronuclear single quantum coherence spectra reveals disruption of the tertiary contacts among the regions close to the active site in the first step of unfolding, i.e., the N-I1 transition. Both of the intermediates, I1 and I2, showed a propensity to self-associate under stirring conditions, but their kinetic profiles are different; the native protein did not show any such tendency under the same conditions. All these observations could have significant implications for the function of the protein.

INTRODUCTION

Peptidyl-prolyl *cis-trans* isomerization, catalyzed by the immunophilin class of proteins, is a ubiquitous process and plays a key role in protein folding and regulation of protein function (1). Cyclophilin, a member of the immunophilins found in all the organisms, including prokaryotes and eukaryotes, is known to be the intracellular receptor of the immunosuppressive drug cyclosporine A (CsA) (2–4). In humans, seven major cyclophilins (from a total of 16 cyclophilins) are expressed, viz., CypA (18 kDa), CypB (22 kDa), CypC, CypD, CypE, Cyp40 (40 kDa), and CypNK (first identified from human natural killer cells). All of these have a conserved domain called cyclophilin like domain (CLD), and some are expressed in combination with other domains. The presence of another domain in combination with CLD depends upon the localization of that particular cyclophilin (1). Several cyclophilins are expressed in yeast as well as in humans, viz., Cpr1–Cpr8, which are different in their size and localization (1). Cpr1 (17 kDa) is homologous to human CypA, which has only a CLD and is expressed in the cytoplasm and nucleus. Cpr2 (20 kDa), Cpr3 (20 kDa), and Cpr5 (23 kDa) are expressed with an amino-terminal signal peptide in addition to the CLD, which directs them to the endoplasmic reticulum (Cpr2 and Cpr5) and mitochondria (Cpr3). Cpr4 (33 kDa) and Cpr8 (35 kDa) are homologous to CypC, and are expressed with a long N-terminal signal peptide, which directs them to vacuoles. Cpr6 (45 kDa) and Cpr7 (45 kDa), expressed with long TPR repeats at the C-terminal, are homologous to human Cyp40. These two cyclophilins are functionally similar to the heat-shock proteins and other protein chaperones (1).

Structures of several cyclophilins from different organisms in both ligand-bound and ligand-free forms have been reported (5–8). The canonical fold of the CLD is well represented by the structure of human CypA (165 amino acids), which consists of an eight-stranded β-barrel surrounded by two helices, one on each face (5–8). It also contains one helical turn with a conserved Trp residue in close proximity to the active site. There is a long loop of ~20 residues between β5 and β6, which is organized in such a manner that the region of the loop comprising residues 64–74 forms a hairpin-like structure close to the active site (5–8).

Submitted October 13, 2016, and accepted for publication December 13, 2016.

*Correspondence: ashutoshk@iitb.ac.in or hosur@tifr.res.in

Editor: Jane Dyson.

http://dx.doi.org/10.1016/j.bpj.2016.12.020

Several efforts to understand the *cis-trans* isomerization of the peptidyl-prolyl bond have been made using different approaches such as NMR line-shape analysis, monitoring changes in R_2 upon substrate binding, crystal structure studies with different peptides, molecular dynamics simulations, and density functional theory calculations (9–13). Eisenmesser and co-workers proposed that the *cis* conformer of the peptide interacts with residues A101, N102, A103, K82, and R55 of the enzyme; afterward, the enzyme catalyzes rotation of the peptide-prolyl bond by 180° to produce the *trans* conformation and makes contacts around residues L98 and S99. During isomerization, the C-terminus of the peptide bond is free to rotate, whereas the N-terminus of the bond remains bound at the catalytic site of the enzyme (9). The authors also concluded that R55 is the key player in *cis-trans* isomerization, which is supported by mutational studies (9,10). Zhao and co-workers proposed the involvement of the guanidino group of the sidechain of R55 in hydrogen bonding with the prolyl nitrogen of the substrate. They also proposed that the isomerization is driven by weakening of the double bond character of the peptide bond (11,12). Camilloni and co-workers proposed the so-called "electrostatic handle mechanism," wherein the enzyme creates an electrostatic environment at the catalytic site that rotates a peptide bond in the substrate by pulling the electric dipole associated with the carbonyl group of the residue preceding proline in the peptide bond (13).

Recently, it was proposed on the basis of the so-called "exact NOE approach" (14,15) that the native state, the so-called "closed state," is in equilibrium with a low-lying excited state, the so-called "open state." (16). In the backbone, these two states differ in six different regions $\beta1$–$\beta2$ (residues 9–16), $\alpha1$ (residues 34–42), $\beta4$ (residues 54–57), the loop between $\beta5$–$\beta6$ (residues 64–78 and 89–94), $\beta6$–$\beta7$ (101–107), and $\beta7$–$\beta8$ (118–127) (16). Of these six regions, four ($\beta4$ and the loops between $\beta5$ and $\beta6$, $\beta6$ and $\beta7$, and $\beta7$ and $\beta8$) are part of the active site. The authors proposed that the peptide substrate binds to the open state, wherein a loop formed by residues 64–74, referred to as the "ligand-binding loop," plays a crucial role in the interaction (16). This suggested that a partially unfolded state is the functionally relevant species for the catalysis. In this context, it becomes imperative to study systematically the unfolding process of the protein.

There have been very few studies on the folding and unfolding pathways of cyclophilins; the unfolding pathways of only two cyclophilins, LdCyp (cyclophilin from *Leishmania donovani*) and PPiA (cyclophilin from *Mycobacterium tuberculosis*), have been reported so far (17,18). The sequence identity of these two proteins with human and yeast cyclophilins is very low. Biophysical characterization from the folding/unfolding point of view has not been done for any of the yeast cyclophilins so far. Therefore, we have undertaken here to study the unfolding pathway of yeast mitochondrial cyclophilin (CPR3), which shows very high sequence identity (~65%) with most of the yeast and human cyclophilins. The results indicate that unfolding of CPR3 proceeds via two intermediates. The intrinsic properties of the two intermediates have also been investigated, which would throw light on the possible fate of the protein inside the cells. The study also revealed that one of the intermediates resembles the so-called functionally relevant "open state" referred to earlier. Subsequent to that study, we have characterized the interaction of CPR3 in the native and one of the intermediate states with a peptide using NMR spectroscopy.

MATERIALS AND METHODS

Protein expression and purification

The cloning, expression, purification, and NMR sample preparation of CPR3 have been reported previously (19), and data have been deposited into the Biological Magnetic Resonance Bank (BMRB: 25832).

Modeling of the protein structure of CPR3 by NMR data

For structural modeling of this protein, we have submitted the chemical shift and sequence file as input at the CS23D2.0 server (http://www.cs23d.ca/). CS23D2.0 uses a combination of maximal sub-fragment assembly, chemical shift threading, shift-based torsion angle prediction, and chemical-shift refinement to generate and refine the protein coordinates (20). To model the complex of the CPR3 with peptide (VHAGPIA), we superimposed the structure of CPR3 and peptide on the crystal structure of the complex of CypA and HIV-1 CA protein (Protein Data Bank (PDB): 1M9C).

Preparation of protein solutions

Samples were prepared at a concentration of 20 μM in buffer (20 mM sodium phosphate (pH 6.5)) with the desired concentration of urea for measurement of the far-ultraviolet (UV) circular dichroism (CD) spectra and intrinsic fluorescence of the protein. NMR experiments were performed at a concentration of 100 μM. Time-dependent changes in structural parameters of CPR3 for 1 M and 4 M urea concentrations were monitored to standardize the incubation time required for achieving equilibrium under these conditions. Under all the conditions studied, the changes occurred within a maximum of 1 h, with no further alterations in the values obtained up to 12 h, suggesting that a minimal time of ~1 h is sufficient for achieving equilibrium. Therefore, we incubated samples at 25°C for 2 h in 20 mM sodium phosphate (pH 6.5).

Far-UV CD spectroscopy

Far-UV CD measurements were carried out on a JASCO (Tokyo, Japan) J-810 spectropolarimeter equipped with a Peltier-type temperature controller and a thermostated cell holder interfaced with a thermostatic bath. Spectra were recorded in a 1-mm-pathlength quartz cuvette, and three scans were accumulated at a scan speed of 100 nm/min at 25°C. The isothermal wavelength scan was recorded in the range 260–198 nm at 25°C, with a response time of 1 s. The final spectra were the average of three scans, and all data were corrected for the baseline contribution of the buffer at all conditions.

The secondary structure of the aggregates was observed using CD spectroscopy at the end of the aggregation reaction (600 h). For recording the CD spectra of the aggregate, the aggregated sample was diluted in water and the spectra were recorded in the same way as described above.

Fluorescence spectroscopy

The intrinsic fluorescence spectra were measured using a JASCO RF-5301PC spectrometer equipped with a Peltier-type temperature controller. The spectra were recorded in a 5-mm-pathlength quartz cuvette, and three scans were accumulated at a scan speed of 100 nm/min. The samples were excited at 295 nm and the emission spectra were recorded in the wavelength range 300–400 nm. The excitation and emission slits were kept at 2.5 and 5 nm, respectively, and the data were recorded at 25°C. The final spectra were the average of all three scans, and appropriate controls for the background emission were subtracted.

Binding of the hydrophobic fluorescent dye anilino-8-naphthalenesulphonate (ANS), with CPR3 was carried out to probe the intermediate conformational states of CPR3 in varying concentrations of the urea denaturant. ANS was added to protein samples (4 μM in 20 mM NaH_2PO_4 buffer (pH 6.5)) with increasing concentration of urea to get a final ANS concentration of 20 μM. The excitation wavelength was 370 nm, and the emission spectra were recorded between 400 and 700 nm. The values were normalized by subtracting the baseline recorded for the probe alone under conditions similar to those used for the experiments.

In the quenching experiment, a stock solution of neutral quencher, acrylamide, was prepared at a concentration of 5 M. The quencher was added to achieve the desired range of quencher concentration (0.1–0.5 M) in the pre-incubated protein sample at four different concentrations of urea (0 M, 2 M, 4 M, and 8 M). The sample was excited at 295 nm, and emission spectra were recorded in the range 300–450 nm. The Stern-Volmer quenching constant was calculated as the slope of the plot of F_0/F values against the input concentration of quencher, acrylamide, in the Stern-Volmer equation,

$$F_0/F = 1 + K_{SV}[Q], \tag{1}$$

where F_0 and F are the fluorescence intensities at an appropriate wavelength in the absence and presence of quencher, respectively, K_{SV} is the Stern-Volmer constant, and [Q] is the concentration of the quencher (21).

Analysis of Intrinsic fluorescence and CD spectra

Data from both fluorescence and CD spectroscopy were converted into the fraction of denaturation by using the equation

$$F_D = (S_{obs} - S_N)/(S_U - S_N). \tag{2}$$

The normalized data were then analyzed quantitatively according to general multi-state transition models. For a two-state model, N↔U, the equation used was (17,22,23)

$$S_{obs} = \left[S_N + S_U e^{-}\left(\frac{\Delta G_{NU}}{RT}\right)\right] \Big/ 1 + e^{-}\left(\frac{\Delta G_{NU}}{RT}\right). \tag{3}$$

Similarly, for a three-state model, N↔I↔U, consisting of one intermediate, I, the native state, N, and the unfolded state, U, the equation used (17,22,23) was

$$S_{obs} = \left[S_N + S_I e^{-}\left(\frac{\Delta G_{NI}}{RT}\right) + S_U e^{-}\left(\frac{\Delta G_{NU}}{RT}\right)\right] \Big/ 1 + e^{-}\left(\frac{\Delta G_{NI}}{RT}\right) + e^{-}\left(\frac{\Delta G_{NU}}{RT}\right), \tag{4}$$

where S_{obs} is the observed signal at a given concentration of denaturant and S_N, S_I, and S_U are the signals due to the native state, the intermediate state, and the unfolded state, respectively. ΔG_{NI} and ΔG_{NU} are the corresponding free energies of the transitions N↔I and N↔U, where ΔG_{NI} and ΔG_{NU} are assumed to have linear dependence on the denaturant concentration, [D], as below,

$$\Delta G_{NI} = \Delta G_{NI}(H_2O) + m_{NI}[D] \tag{5}$$

$$\Delta G_{NU} = \Delta G_{NU}(H_2O) + m_{NU}[D] \tag{6}$$

Size-exclusion chromatography

Size-exclusion chromatography (SEC) has been used to study urea-induced unfolding of CPR3. Experiments were carried out with a Superdex-75 column (V_0 = 8.75 mL) using an ÄKTA pure FPLC (GE Health Care, Little Chalfont, United Kingdom). The column was washed with filter-sterilized degassed MilliQ and pre-equilibrated with the buffer with the desired concentration of urea, and a 500 μL volume of the 40 μM concentration sample was injected into the column at a flow rate of 0.5 mL/min. The eluent was detected online by absorbance at 280 nm. In the case of urea-denatured protein, the column was equilibrated with the defined concentration of urea dissolved in buffer. We used a set of globular proteins with known molecular weights for calibration of the column, viz., conalbumin (75 kDa), bovine serum albumin (66 kDa), ovalbumin (43 kDa), carbonic anhydrase (25 kDa), and ribonuclease A (13.7 kDa).

The fraction of molecules that undergo the transition from a compact to a less compact state is determined by the formula (24,25)

$$F_{LC} = \frac{S_{LC}}{(S_C + S_{LC})}, \tag{7}$$

where S_C and S_{LC} are the peak areas of the compact and less compact states, respectively. The fraction of the unfolded state (F_U) is calculated by the equations (24,25)

$$F_U = F_{LC}(V_{LC} - V_{PF})/(V_U - V_{PF}) \tag{8}$$

$$V_{LC} = V_{PF} + (F_U/F_{LC})(V_U - V_{PF}). \tag{9}$$

V_{LC}, V_{PF}, and V_U are the elution volume of the less compact state, the partially folded (PF) state, and the unfolded state, respectively. V_U at any given urea concentration is estimated from the baseline extrapolated from the urea dependence of the elution volume for unfolded molecules. V_{PF} can be roughly estimated as the maximal value of elution volume for less compact molecules.

The fractions of I1 and I2 are evaluated by using the equations

$$F_{I1} = F_D - F_{LC} \tag{10}$$

$$F_{I2} = F_{LC} - F_U. \tag{11}$$

NMR spectroscopy

NMR spectra were recorded with 100 μM protein samples in 20 mM NaH_2PO_4 (pH 6.5), 150 mm NaCl, and 10% (v/v) ^{2}H2O on a Bruker (Billerica, MA) Ascend 750-MHz spectrometer equipped with a Z-gradient room temperature probe, at 25°C. The two-dimensional ^{15}N heteronuclear single-quantum correlation (HSQC) spectra were recorded in different concentrations of denaturant urea (0 M, 0.5 M, 1.0 M, 1.5 M, 2.0 M, 3.0 M, 4.0 M, and 8.0 M). The HSQC spectrum for each case was acquired with 2048 and 256 complex points in the ^{1}H and ^{15}N dimensions, respectively, and with 16 scans. Spectra were processed by using the software Topspin 3.2.

Chemical-shift perturbations (CSPs) were analyzed to check the effect of 2 M urea and peptide binding on each residue of the protein. The combined CSP Δ_{Total} of $^1H^N$ and ^{15}N nuclei were weighted as

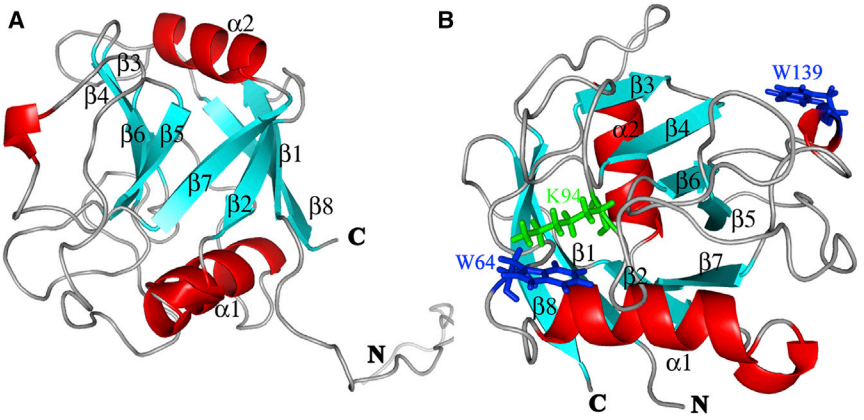

FIGURE 1 (*A*) Structure of CPR3 highlighting the secondary structures. The β-strands correspond to residues K23–V30 (β1), G36–L42 (β2), R73–I75 (β3), M79–Q81 (β4), G114–S118 (β5), F130–I132 (β6), H144–V150 (β7), and E173–E181 (β8); α-helices correspond to residues K49–T59 (α1) and M154–S162 (α3); and the helical turn corresponds to residues P138–L140. Helices, strands, and loops are shown in red, cyan, and gray, respectively. (*B*) Structure of CPR3, highlighting the positions of tryptophan residues. Stick representations of two tryptophan residues are shown in blue, and one Lys residue close to the sidechain of one Trp (W64) is shown in green. To see this figure in color, go online.

$\Delta_{Total} = ((\Delta^1H)^2 + (0.2\times\Delta^{15}N)^2]^{1/2}$ to normalize the larger chemical-shift range of ^{15}N (26,27). The resonance frequencies at pH 6.5 of CPR3 in the absence of urea and peptide were taken as reference points. In the interaction study, ^{15}N-HSQC experiments were recorded at different ratios of protein to ligand (1:0, 1:1, 1:2, 1:4, 1:6, 1:8, 1:10, 1:20, and 1:30).

Aggregation kinetics

The process of aggregation was initiated by continuous stirring (230 rpm) of the protein (100 μM) in 2 M and 4 M urea solutions at 37°C. The aggregation kinetics was followed using ThT assays: 60 μL of each sample was added at regular time intervals to 2.94 mL of 10 μM ThT solution, and the ThT fluorescence of the resulting samples was measured between 450 and 600 nm at 25°C with the excitation wavelength fixed at 444 nm.

The kinetic parameters of aggregation reaction were calculated by fitting kinetic traces to the sigmoidal equation (28)

$$F = F_0 + m_0 t + \frac{F_1 + m_1 t}{1 + e^{-\left[\left(t - t_{1/2}\right)/\tau\right]}}, \qquad (12)$$

where F_0 and F are the observed ThT fluorescence ratios at time zero and time h, respectively; $t_{1/2}$ is the time taken to reach 50% of the maximal fluorescence; m_0 and m_1 are the slopes of the pre- and post-transition regions, respectively, of the aggregation profiles; and τ is the apparent time constant. The apparent rate constant (k_{app}) and lag time (t_{lag}) are calculated as $k_{app} = 1/\tau$ and $t_{lag} = t_{1/2} - 2\tau$.

Congo red difference spectroscopy

Aliquots of 60 μL of each sample were mixed with 2.94 mL of solutions containing 20 μM Congo red (CR), 20 mM phosphate buffer, and 150 mM NaCl (pH 6.5), at 25°C. After a 2- to 3-min equilibration, absorption spectra were acquired from 400 to 700 nm. The difference spectra were obtained by subtracting the spectra of CR alone and fibrils alone from the spectrum of the CR and fibril complex.

Atomic force microscopy

Morphology of the fibrils formed at the end of the aggregation reaction (600 h) was observed using atomic force microscopy (AFM) (Asylum Research, Santa Barbara, CA). Small aliquots of the aggregation reactions were taken and diluted to a final concentration of 20 μM. The samples were then spotted on a freshly cleaved mica sheet and incubated at room temperature for 5–10 min. A subsequent washing with double distilled water was done to remove the unbound aggregates. The washed samples were then dried at room temperature for 40 min. AFM imaging was performed in tapping mode with a silicon nitride cantilever. The scan rate was kept at 1 Hz and two to three different areas were randomly scanned. Oligomer sizes were measured from the heights in cross sections of the topographic AFM images.

RESULTS

Structural features of native CPR3

We have used the CS23D2.0 server (http://www.cs23d.ca/) to model the structure of CPR3 from chemical-shift data (BMRB: 25832) (19,20). The calculated structure is validated by the PSVS server (http://psvs-1_5-dev.nesg.org/). The Ramachandran plot statistics for the most favored, additionally allowed, generously allowed, and disallowed regions are 88.7%, 11.3%, 0.0%, and 0.0%, respectively. The structure of CPR3 so derived possesses a canonical cyclophilin fold comprised of eight antiparallel β-strands, two α-helices, and one helical turn (Fig. 1 *A*). The eight β-strands are arranged in the order β1-β8-β3-β4-β6-β5-β7-β2, and they form a β-barrel surrounded by two helices, one on each face (Fig. 1 *A*). This secondary structure correlates well with the secondary structure previously predicted using the TALOS+ program (19,29). CPR3 shows high sequence identity with the CPR1 from yeast (~70%) and CypA from humans (~65%). The three-dimensional structure of CPR3 has backbone root mean-square deviations (RMSDs) of 0.24 Å and 0.67 Å with respect to CPR1 (PDB: 1VDN) and CypA (PDB: 1OCA), respectively, which suggests that the modeled structure is acceptable. In CPR3, there are two tryptophan residues at positions 64 and 139. Of these, W139 is well conserved in all cyclophilins, whereas W64 is replaced by a phenylalanine residue in most other cyclophilins, with the exception of CPR2, where it is replaced by a lysine residue. Residue W64 is present at the loop formed between α1 and β3, whereas W139 is present at the helical turn (Fig. 1 *B*). The indole ring of these two tryptophan residues is only partially projected toward the core of the protein molecule, and therefore, the two

tryptophans seem to be partially exposed in the structure of CPR3.

Urea-induced unfolding of CPR3 studied by optical methods

Spectroscopic studies of CPR3 in the presence of increasing urea concentrations were performed to analyze the effect of denaturant on its structural properties. The spectral parameters of the tryptophan fluorescence emission, such as position, shape, and intensity, are dependent on the electronic and dynamic properties of the chromophore environment; hence, steady-state tryptophan fluorescence has been extensively used to obtain information about the structural and dynamical properties of proteins (30). In this case, modification of the microenvironment of tryptophan residues of CPR3 due to denaturants was monitored by studying changes in the intensity and/or wavelength of emission maxima (λ_{max}) of tryptophan fluorescence as a function of denaturant concentration. Changes in the λ_{max} of tryptophan fluorescence of CPR3 with increasing urea concentration are shown in Fig. 2 *A*. For native CPR3, significant tryptophan fluorescence was observed with emission λ_{max} at 343.5 $\pm$ 0.5 nm, which is comparable to the fluorescence emission λ_{max} (341–345 nm) of partially exposed tryptophan residues (30–33). Hence, in native CPR3, the tryptophan moieties are partially exposed from the hydrophobic core of the protein, which is also consistent with the positions of tryptophans observed in the structure. Between 0 M and 4 M urea, quenching of tryptophan fluorescence intensity along with a red shift in λ_{max} of the native enzyme was observed (Figs. 2 *B* and S1 in the Supporting Material). Afterward, with an increase in urea concentration from 4 M to 8 M, a significant enhancement in the tryptophan fluorescence, along with a red shift in λ_{max} to ~354 $\pm$ 0.5 nm, was observed (Figs. 2 *B* and S1). This unusual behavior of an initial decrease and subsequent increase of fluorescence can be explained by the structure of the protein as follows. In the 0–4 M urea range, K94 remains in close proximity to W64, as in the native structure, and quenches the latter's fluorescence (Fig. 1 *B*). Beyond 4 M urea, due to unfolding, this quenching effect is removed, resulting in enhanced fluorescence.

Far-UV CD studies on urea-induced unfolding of CPR3 were carried out to study the effect of urea on the secondary structure of the enzyme. Far-UV CD of the native protein exhibited a pronounced minimum at 226 nm, characteristic of a protein with prevalent β-sheets. The effect of increasing

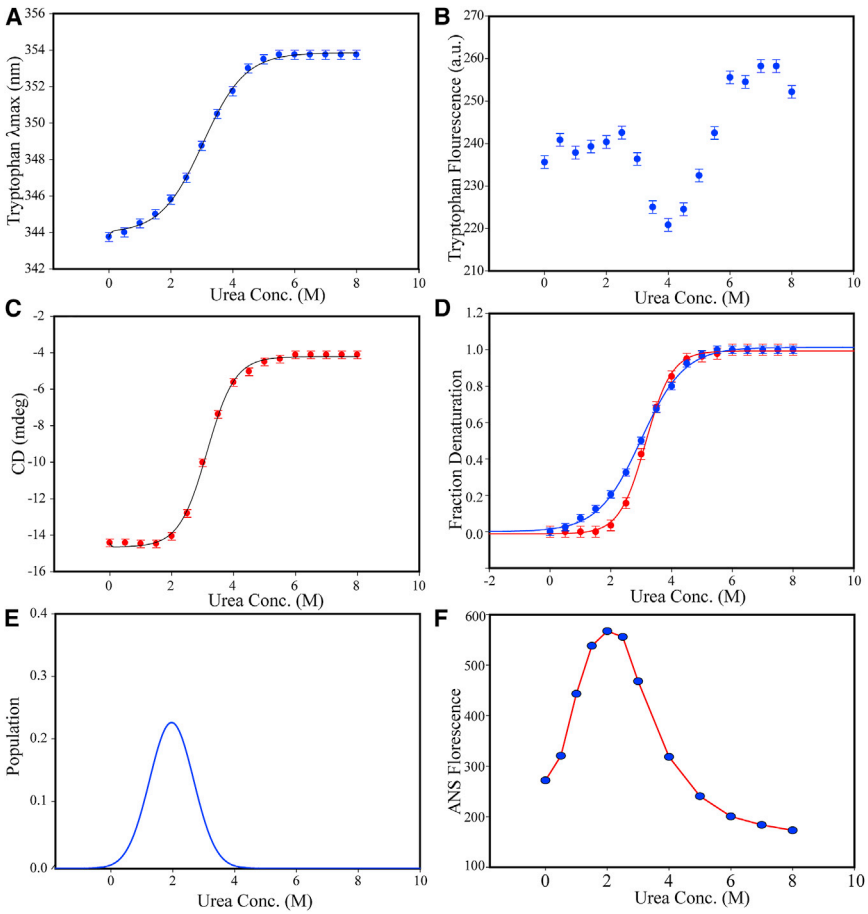

FIGURE 2 Urea-induced unfolding of CPR3 studied by fluorescence and CD spectroscopy. (*A*) Urea-induced unfolding followed by monitoring of the tryptophan fluorescence λ_{max} for tertiary structure. (*B*) Urea-induced unfolding followed by monitoring of the tryptophan fluorescence intensity. (*C*) Urea-induced unfolding followed by CD ellipticity at 226 nm for secondary structure. (*D*) Normalized transition curves for urea-induced unfolding of CPR3 as followed by CD ellipticity at 226 nm (θ_{226}) for secondary structure and by relative tryptophan fluorescence λ_{max} at different urea concentrations for tertiary structure. A linear extrapolation of the baselines in the pre- and post-transitional regions was used to determine the fraction of unfolded protein within the transition region by assuming a two-state mechanism of unfolding. The curves for CD and fluorescence are red and blue, respectively. (*E*) The population curve for urea-induced unfolding, in which the difference in the normalized value of λ_{max} and θ_{226} is plotted against urea concentration. (*F*) Plot of ANS fluorescence at 470 nm after excitation at 370 nm with increasing urea concentration. To see this figure in color, go online.

urea concentration on the ellipticity at 226 nm (θ_{226}) is summarized in Fig. 2 *C*. Up to a urea concentration of ~2 M, no significant change in ellipticity at 226 nm was observed. However, in the range 2–6 M urea, a gradual reduction was found in the overall secondary structure, with almost complete loss of ellipticity at 6 M urea.

Changes in the molecular properties of CPR3 such as CD ellipticity at 226 nm (θ_{226}) and tryptophan fluorescence emission λ_{max} with increasing urea concentration showed a cooperative process, but the data obtained from these two independent probes were non-superimposable (Fig. 2 *D*). This seems to suggest the presence of at least one intermediate in the unfolding process. To further quantitate this, noting that the two curves have the appearance of a two-state unfolding, we tried to fit our data with two-state models using Eq. 3. Both CD and fluorescence data fitted reasonably well. $\Delta G_{NU}(H_2O)$ and m_{NU} values derived from CD data were 4.22 and −2.25 kcal mol^{-1}, respectively; and corresponding values for fluorescence measurements were 2.562 and −1.42 kcal mol^{-1}, respectively. Clearly, the two results are different, considering that urea-induced unfolding of CPR3 is a multiphasic process with presence of equilibrium intermediate/intermediates (22,23,34,35) (Fig. 2 *D*). We also tried to fit both sets of data to Eq. 4 for a three-state unfolding, but this fitting was poor and unreliable. It also appears, from the curve in Fig. 2 *D*, that tertiary-structure disruption starts quite early (~0.5 M), whereas the secondary-structure disruption starts relatively later (~2.5 M) with increasing urea concentration. We plotted the difference of the normalized-fraction denaturation of tertiary and secondary structure, known as the population curve, against urea concentration to find the denaturant concentration at which intermediates are maximally accumulated in the unfolding pathway (Fig. 2 *E*). The population curve clearly shows the existence of an equilibrium intermediate maximally accumulated at 2 M urea. The CD and fluorescence data in Fig. 2, *B* and *D*, also hint at the presence of one more intermediate state at ~4 M urea: first, the unfolding curves obtained from the CD and fluorescence do not superimpose (small difference); and second, as seen in Figs. 2 *B* and S1, the tryptophan fluorescence intensity decreases up to 4 M urea and then starts increasing. This latter observation is suggestive of a structural change around 4 M urea, as explained earlier, which points to the presence of another intermediate in the unfolding process (36). Thus, these optical methods identify the four-state reaction of urea-induced unfolding of CPR3 with the presence of two intermediates.

ANS fluorescence study

Next, we performed ANS binding studies, which have been used for identification and characterization of folding intermediates and the molten globule state in general (25,34,35). ANS fluorescence first gradually increases with the increase in urea concentration between 0 M and 2 M; thereafter, it gradually decreases up to 6 M urea (Fig. 2 *F*). Maximal ANS binding was observed at 2 M urea concentration, with an ~2.5-fold increase in emission intensity suggesting increased exposure of the hydrophobic surface compared to the native structure. Above 2 M urea concentration, the protein showed a gradual decrease in ANS binding, which is an indication of disruption of hydrophobic patches due to unfolding. Thus, ANS binding further suggests the existence of an intermediate in the unfolding pathway of CPR3, which is maximally accumulated at 2 M urea.

Urea-induced unfolding of CPR3 studied by SEC

SEC is a wonderful technique for identifying intermediates in the unfolding process (37,38). It has also been used to obtain the hydrodynamic data of the intermediates, as well as to observe changes in the molecular dimension in N↔I and I↔U transitions (37,38). In the case presented here, the study of urea-induced unfolding of CPR3 by SEC suggested the existence of two intermediates in the unfolding pathway. SEC profiles of the CPR3 at different concentrations of urea are shown in Fig. 3 *A*. In the case of CPR3, an "all or none transition" was observed from a compact (at high elution volume with a small molecular dimension) to a less compact state (low elution volume with a large molecular dimension), which is suggested by a bimodal distribution of the protein elution volume in the transition region (2–4 M). The SEC data for CPR3 are comparable to previously reported SEC data for carbonic anhydrase and β-lactamase, which have two intermediates in the unfolding pathway (24,25).

A detailed analysis of the SEC data is given in Materials and Methods. Plots of the dependence of the elution volumes of compact and less compact states on urea concentration are shown in Fig. 3 *B*. The maximal elution volume of the compact state corresponds to the native state, denoted by N. The elution volume of the compact state continues to decrease up to a certain urea concentration, i.e., 4 M urea, at which all compact molecules disappear. A comparison of these SEC data for CPR3 with similar data on carbonic anhydrase and β-lactamase (24,25) suggested that the curve of the compact state reflects the transition from the native to the expanded compact state (I1) to the partially folded/less compact state (I2).

The urea dependence of the parameters F_{LC}, F_U, and F_D are plotted in Fig. 3 *C*. Clearly, the curves for F_{LC} and F_U (derived from SEC) are non-superimposable with each other or with that of F_D (derived from intrinsic fluorescence) (Fig. 3 *C*). This suggests the existence of three different stages of unfolding of CPR3, with two intermediates. From these fractional populations of the two intermediates, F_{I1} and F_{I2}, have been calculated from Eqs. 10 and 11 as described in Materials and Methods. A plot of the fractions of intermediate states, F_{I1} and F_{I2}, as a function of urea

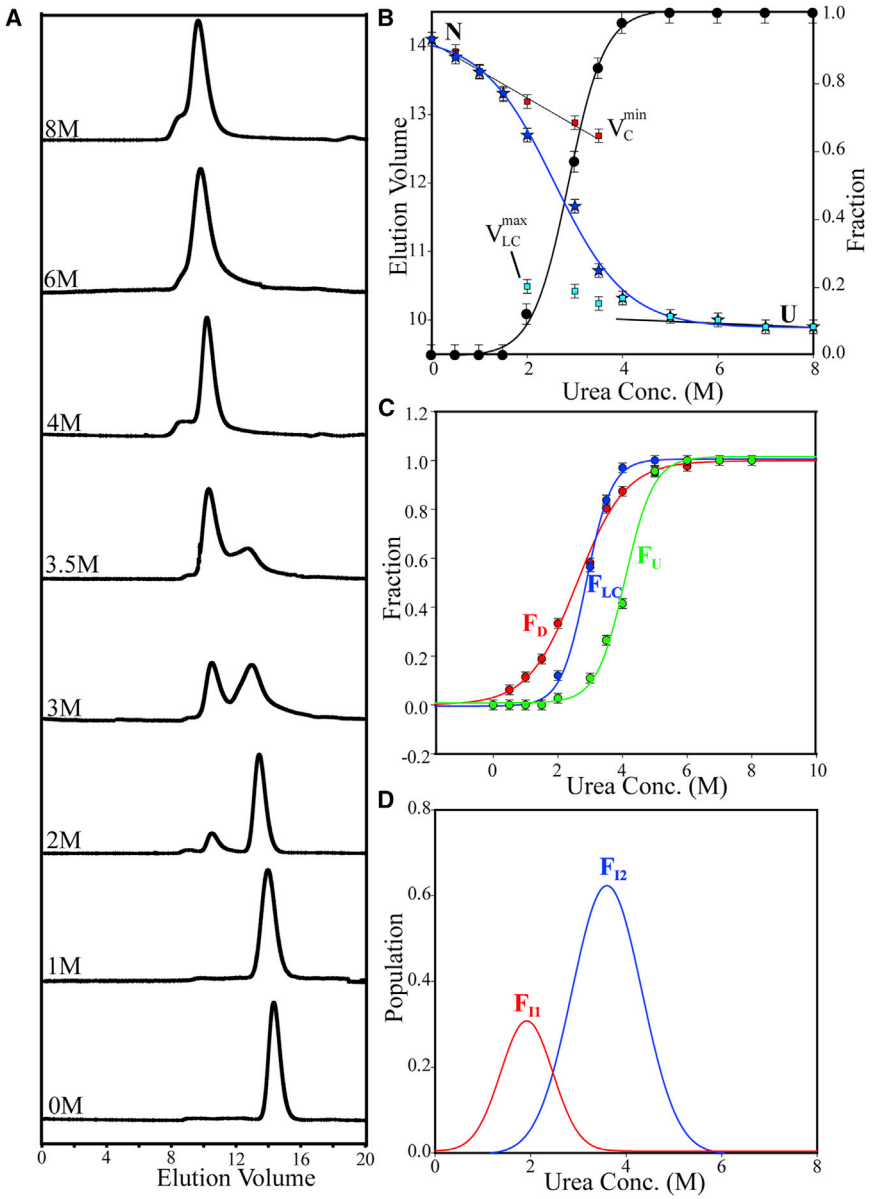

FIGURE 3 Urea-induced unfolding study of CPR3 by SEC. (*A*) Elution profiles of CPR3 at different urea concentrations. (*B*) Dependence of elution volumes of compact, V_C, and less compact, V_{LC}, states with increasing urea concentration, shown by red and cyan squares, respectively. The urea dependence of the average elution volume, V_{el} (*blue curve*), calculated from V_C and V_{LC} using the equation $V_{el} = [1 - F_{LC}] \times V_C + F_{LC} \times V_{LC}$. The urea dependence of the fraction of less compact molecules (F_{LC}) is shown in black. (*C*) The fraction of the denatured state (F_D) obtained from the fluorescence study, and the fractions of the less compact state (F_{LC}) and the unfolded state (F_U) obtained from SEC are shown in red, blue, and green, respectively. (*D*) Population curves for the I1 and I2 states (*red* and *blue curves*, respectively) in terms of the fractions in the N-U transition. To see this figure in color, go online.

concentration is shown in Fig. 3 *D*, which reflects the progressive changes as the protein unfolds with increasing urea concentration. It can be seen that I1 and I2, in the unfolding pathway of CPR3 are maximally populated at 1.9 M and 3.8 M urea, respectively (Fig. 3 *D*).

Thus, taking these data together, we conclude that the urea-induced unfolding pathway of CPR3 is a four-state process with the presence of two intermediates, I1 and I2, maximally populated at ~2 M and ~4 M urea, respectively.

Characterization of the intermediate states

For the characterization of the intermediate states of the protein, we used different biophysical tools including NMR spectroscopy. In CPR3, at 2 M urea, a change in tryptophan fluorescence emission λ_{max} without any change in the far-UV CD spectrum was observed with respect to the native state, which suggests that the N-I1 transition is accompanied by a considerable loss of tertiary structure, with conservation of the entire secondary structure (Figs. 2 *E* and 4 *A*). The far-UV CD data and the emission data also suggest that CPR3 at 4.0 M urea has considerably less secondary and tertiary structure (Fig. 4 *A*). In the ANS binding study, maximal ANS binding was observed at 2.0 M urea as a result of maximal exposure of the hydrophobic surface, whereas at 4.0 M urea, weak ANS binding was observed due to substantial unfolding (Fig. 2 *F*).

The Stern-Volmer coefficient (K_{SV}) of a protein in the different states is a very sensitive and important probe for determining the extent of exposure of tryptophan residues

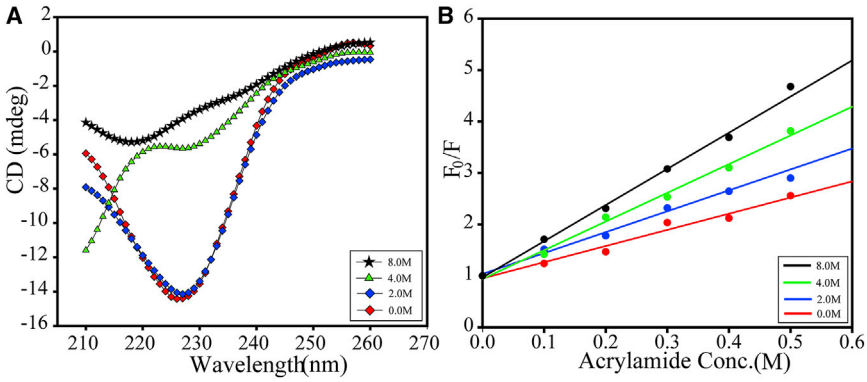

FIGURE 4 Characterization of intermediates formed in the unfolding pathway. (*A*) CD spectra of CPR3 in all four states, N (0 M urea), I1(2 M urea), I2 (4 M urea), and D (8 M urea), in the unfolding pathway. (*B*) The Stern-Volmer plot of acrylamide quenching for CPR3 for the four states. To see this figure in color, go online.

in solution (17,21,30). Fig. 4 *B* shows a Stern-Volmer plot at 0 M, 2 M, 4 M, and 8 M urea for all four states. The K_{SV} values for CPR3 at 2 M and 4 M urea were found to be 4.06 M^{-1} and 5.57 M^{-1}, respectively, which are higher than that of the native state (3.14 M^{-1}). This quenching is accompanied by a red shift in the λ_{max} of emission. The K_{SV} value of the denatured state of CPR3 (8 M urea) was found to be 7.02 M^{-1}, which is significantly higher than that of either the native or the I1 or I2 states. These results consolidate intermediate exposure of tryptophan in the I1 and I2 states.

The native, intermediate, and unfolded states of the protein were further characterized by NMR spectroscopy. The ^{15}N-HSQC spectrum of the native state is well dispersed and shows characteristics of well folded monomeric proteins (Fig. 5 *A*). The ^{15}N-HSQC spectrum of CPR3 at 2 M urea is similar to that of the folded monomeric protein; but some peaks are shifted, suggesting some disruption of the tertiary structure in the protein (Fig. 5 *B*). The ^{15}N-HSQC spectrum of CPR3 at 4 M urea is more suggestive of an unfolded protein, showing most peaks between 7.6 ppm and 8.6 ppm (narrow dispersion); however, some peaks

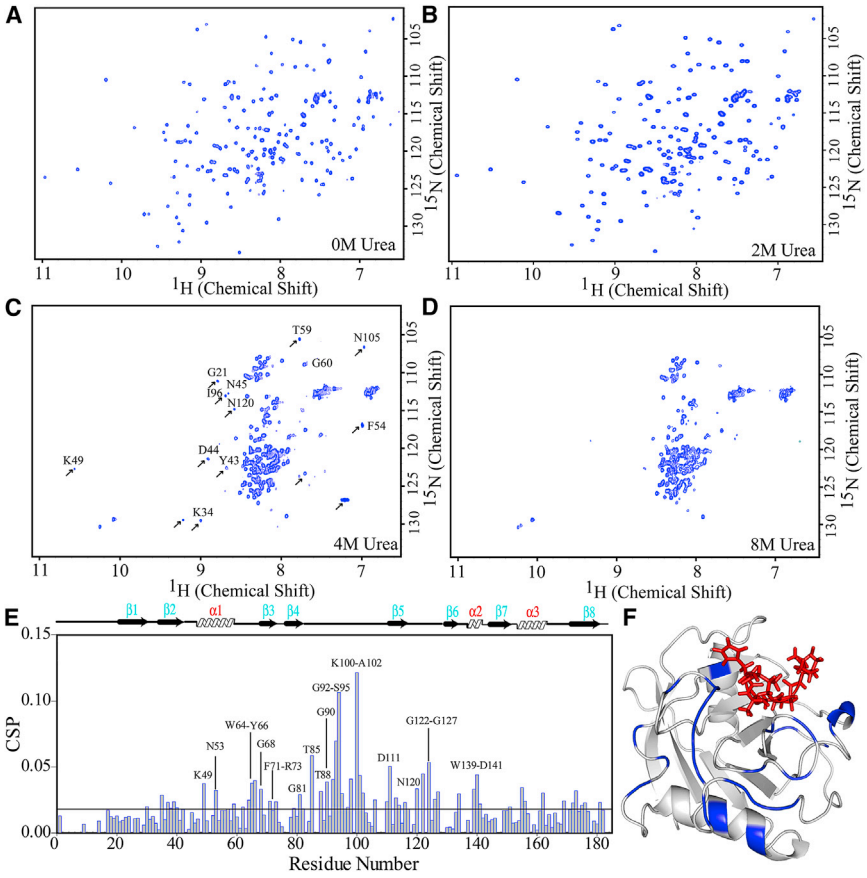

FIGURE 5 (*A–D*) NMR spectroscopy of the ^{15}N-HSQC spectra of the four states, N (0 M urea), I1 (2 M urea), I2 (4 M urea), and D (8 M urea). In (*C*), some peaks are marked by arrows to show that they belong to the native-like structure. Peaks having almost identical chemical shifts are labeled. (*E*) Plot of residue-wise CSPs of CPR3 in the I1 state with respect to the native state. (*F*) Ribbon representation of CPR3 in complex with the VHAGPIA peptide, showing residues with high CSP in the I1 state in blue. The VHAGPIA peptide is shown in red stick representation. To see this figure in color, go online.

were also observed in the spectrum beyond 7.6–8.6 ppm, indicating the presence of some residual structure (Fig. 5 *C*). The denatured-state spectrum (at 8 M urea) shows that the protein is completely unfolded (Fig. 5 *D*).

Overlap of the ^{15}N-HSQC spectra of CPR3 at 0 M and 2 M, depicted in Fig. S2, shows a pronounced change in the chemical shift for some of the residues at 2 M urea. CSPs were calculated to identify the residues involved in the N-I1 transition. We used urea titration (0 M, 0.5M, 1.0 M, 1.5 M, and 2.0 M) to transfer the assignment from 0 M urea to 2 M urea (data not shown). Significant CSPs were observed for residues K49, N53, W64–Y66, G68, F71–R73, T88, G90, G92–K94, Y97–G98, K100–A102, D111, A113, N120, G122, N124, N126, and W139–L140. Most of the residues (except K49 and N53) are found to be in the loop regions of the protein, which are involved in the formation of the peptide binding cleft. These residues correspond to the residues of CypA, which are well known for peptide binding and catalysis. A plot of the CSPs versus residue number and a cartoon of CSPs projected onto the structure of CPR3 are shown in Fig. 5, *E* and *F*, respectively. In the ^{15}N-HSQC spectrum at 4 M urea, some of the peaks observed beyond the central region seem to belong to α1 and regions close to α1, which suggests that in the I2 state, the α1 helix has been partly retained in its structure (Fig. 5 *C*).

In addition to the unfolding study, we also performed a refolding study using solution NMR. For the refolding study, the native protein was first incubated in 8 M urea for 2 h; afterward, we performed exhaustive dialysis at the 0.25 mg/mL protein concentration in the native-state buffer (50 mM NaH_2PO_4 and 150 mM NaCl (pH 6.5)). Comparison of the ^{15}N-HSQC spectrum of the refolded protein with that of the native protein suggested that refolded CPR3 is identical to native CPR3 (Fig. S3). Therefore, CPR3 is capable of folding reversibly.

Aggregation potency of CPR3 along the unfolding pathway

Protein misfolding or partial unfolding and consequent aggregation, if any, has serious implications for biological functions. To see whether the native and intermediate states along the unfolding pathway of the protein are aggregation prone, we induced the aggregation process by standard procedures and monitored the process by thioflavin T (ThT) fluorescence. The aggregation was initiated by stirring the protein (100 μM) solution at 37°C. We observed that the native protein had no tendency to aggregate under the conditions used (data not shown), whereas the I1 and I2 states did show a tendency to aggregate. Fig. 6 *A* shows kinetic traces of I1 and I2 aggregation. Both kinetic curves show lag-phase kinetics and can be fitted to a sigmoidal function described by Eq. 12, suggesting that the aggregation kinetics is in agreement with the nucleation-dependent polymerization mechanism (Fig. 6 *A*) (39,40). The aggregation kinetic parameters, such as lag time (τ_{lag}), apparent rate constant (k_{app}), and amplitude, were calculated using Eq. 12, as described in Materials and Methods. The τ_{lag} values for I1 and I2 intermediates were found to be 376.6 h and

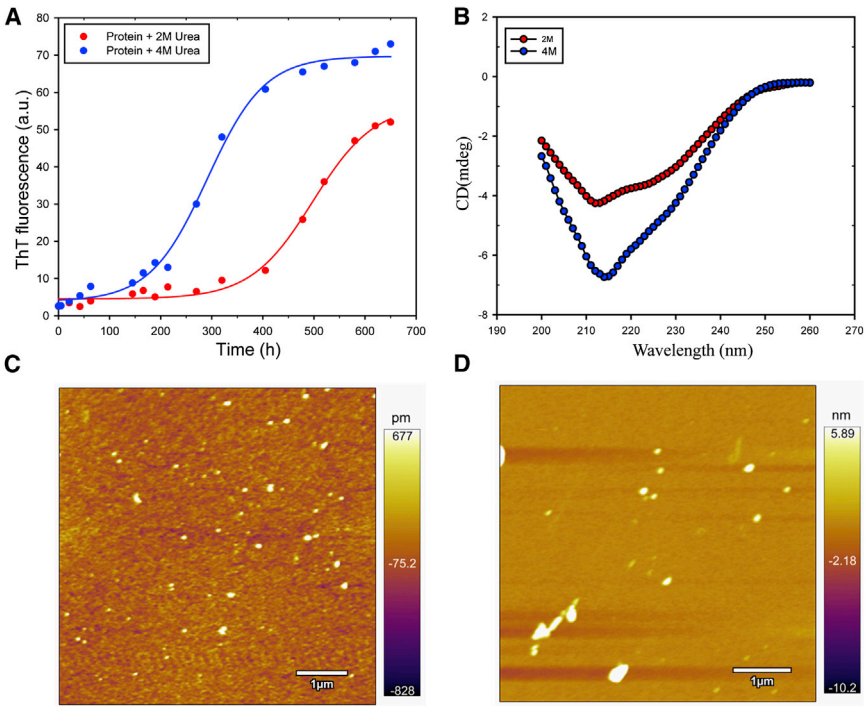

FIGURE 6 Aggregation kinetics of the I1 and I2 states of the protein. (*A*) Aggregation kinetics of the I1 (*red*) and I2 (*blue*) states. (*B*) CD spectra of I1 and I2 in the aggregated state. (*C* and *D*) AFM images of the aggregated I1 and I2states, respectively. To see this figure in color, go online.

179.4 h, respectively. This indicated that the nucleation of aggregation of the I1 intermediate is ~109% slower than that of the I2 state. However, k_{app} values were similar: 0.017 h^{-1} and 0.019 h^{-1} for the I1 and I2 states, respectively. The amplitude of the kinetic curve of the I2 state (~66 a.u.) was slightly higher than that of the I1 state (~52 a.u.) (Fig. 6 *A*). Taken together, these data suggest that the I2 state, which contained a markedly lower content of secondary structure compared to the I1 state, aggregated faster. This might be due to the fact that the unfolded state, as compared to the folded state, can easily reorganize into cross-β structure. On the other hand, the folded intermediate state has to first unfold to form cross-β structure.

The morphologies of the aggregates formed by the two intermediates were assessed using non-contact-mode AFM. Fig. 6, *C* and *D*, shows AFM images of the two aggregates. The analysis showed many species with height values of ~15 nm and ~100 nm for the aggregates formed from the I1 and I2 states, respectively. Since spherical oligomers observed here showed a marked increase in ThT fluorescence (Fig. 6 *A*), it appears that they are amyloid-like oligomers. Similar spherical oligomers have been observed in many other systems (41–43). We also analyzed the secondary structural status of the two aggregates by far-UV CD (Fig. 6 *B*). The far-UV CD spectrum of the aggregates formed by the I1 state showed two negative bands at 212.5 nm and 226.0 nm, whereas the spectrum of the aggregate formed by the I2 state showed a dominant negative CD band at 214 nm and a weak band at ~226 nm. These indicate that the predominant secondary structure of both the aggregates is extended β-sheets. However, the presence of residual α-helices present in the precursors cannot be ruled out. As revealed by negative ellipticity between 226 and 210 nm, the aggregate of the I2 state contains higher secondary structure than the aggregate of the I1 state.

To evaluate whether the oligomers possess a cross-β motif, a hallmark of amyloid fibrils, we also assayed our aggregates with CR binding. CR binds with fibrillar aggregates and gives information about the cross-β motif (40,41,44). The CR difference spectra, calculated by subtracting the spectra of CR alone and aggregate alone from those of the aggregates in the presence of CR, showed maxima at 540 nm (data not shown). The CR difference spectrum with a maximum at 540 nm is a characteristic of CR binding to the cross-β motif (40,41,44). We also observed that a change in the CR absorbance of the I2-state aggregate at 540 nm is larger than that of the I1-state aggregates, indicating that the former contains more cross-β motif. This observation agrees with our far-UV CD data. Taken together, the data presented above show that both structured and unfolded intermediates of cyclophilins convert into stable oligomers. Both the oligomers possess the ability to bind fibril-specific dyes such as ThT and Congo red, although to a lesser extent than the mature fibrils.

Interaction of VHAGPIA peptide with the native and I1 states of CPR3

Since in the previous reports weak binding affinity was reported between cyclophilins and peptide, with a dissociation constant in the millimolar range (13), we used NMR, which is a very useful technique for characterization of such weak interactions (45,46). Here, we used the heptapeptide fragment (VHAGPIA) from the HIV 1-CA protein (5) and studied its interaction with CPR3 by monitoring the CSPs and peak intensity changes in the ^{1}H-^{15}N HSQC spectrum of the protein. We recorded ^{15}N-HSQC spectra at different ratios of CPR3 to peptide (1:0, 1:1, 1:2, 1:4, 1:6, 1:8, 1:10, 1:20, and 1:30). The changes in chemical shifts of some of the residues at different ratios are shown in Fig. 7 *A*, and a plot of CSPs and normalized changes, in intensity against residue number are shown in Fig. 7, *B* and *C*, respectively.

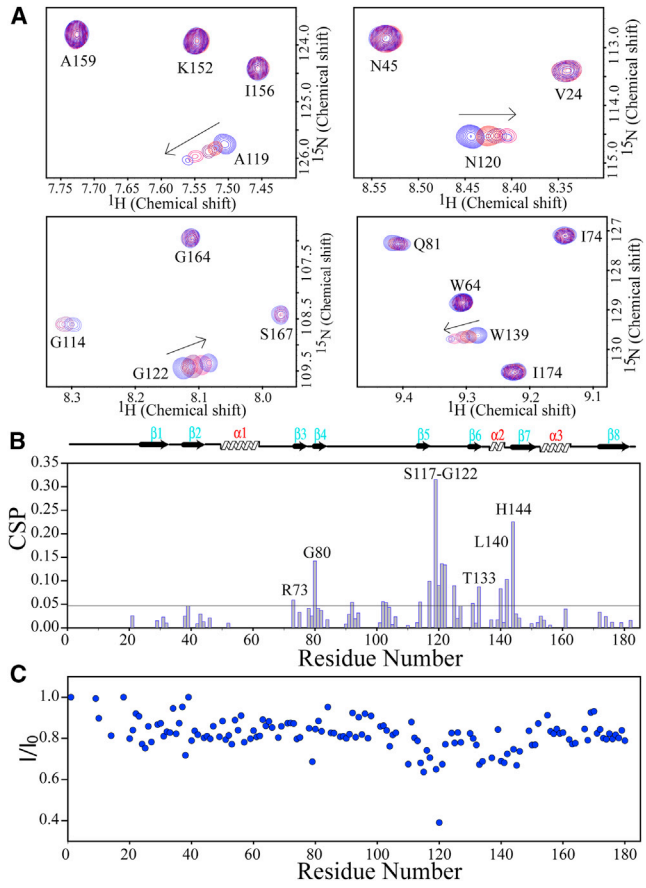

FIGURE 7 Interaction of CPR3 with the peptide (VHAGPIA) as studied using NMR spectroscopy. (*A*) Extracts of different regions of the superimposed ^{15}N-HSQC spectra of CPR3 in the absence of peptide (*blue*) and in the presence of different equivalents of peptide (1:6 (*red*); 1:10 (*brown*); 1:20 (*pink*); and 1:30 (*blue*)). Movement of the peak with increasing peptide concentration is shown by the arrow. (*B*) Residue-wise CSP plot of ^{15}N-HSQC NMR signals of CPR3 in the presence of 30 equivalents of peptide. (*C*) Residue-wise normalized I/I_0 profiles of the ^{15}N-HSQC NMR signals of CPR3 in the presence of 30 equivalents of peptide. To see this figure in color, go online.

We observed, in general, that some residues exhibited distinct CSPs, whereas others exhibited only intensity changes. CSPs indicate structural changes due to binding, and fast chemical exchange between bound and free protein compared to the chemical-shift change (in Hz) on binding. Intensity changes reflect line broadening due to intermediate exchange between the bound and free protein. Significant CSPs (>0.05) were observed for residues R73 (β3), I80 (β4), S117 (β5), A119–G122, T125 (loop between β5 and β6), T133, L140, G142 (the loop between β6 and β7), and H144 (β7). Peak intensity changes were observed for residues M79 (β4), H110, G114–L115 (β5), A119–A121 (the loop between β5 and β6), T133–T134, C137, L140–G142 (the loop between β6 and β7), and H144–V146 (β7). Overall, it appears that residues participating in peptide binding are found in six clusters: β3, β4, β5, the loop between β5 and β6, the loop between β6 and β7, and β7. From quantitative analysis, it appears that of all these regions, two loops, one between β5 and β6 (A119–G122) and another between β6 and β7 (L140–L142), are the most important regions for the interaction. At low equivalents of CPR3 and peptide (1:4), CSPs were first observed for residues A119 and N120 (equivalent to A101 and N102 of CypA from humans); and at high equivalents (1:30), the highest intensity change was observed for residue N120 (Fig. 7, *B* and *C*). We also observed the interaction of CPR3 incubated at 2 M urea with peptide at a 1:10 ratio. Comparison of CSPs for the native state witih those at 2 M urea of CPR3 of the same residues suggested that the binding of CPR3 at 2 M urea with peptide is weaker compared to that with the native state, which suggests that the new population (I1 state) at 2 M urea does not bind with the peptide (Fig. 8).

DISCUSSION

The structural fold of cyclophilins is well conserved in all organisms, including prokaryotes and eukaryotes, even though their sequence identity is very low. As the amino acid sequence holds the key for a protein to adopt its native structural folds, differences in unfolding pathways in different cyclophilins can be expected. Unfolding pathways have been studied for cyclophilins from *Leishmania donovani* (LdCyp) and *Mycobacterium tuberculosis* (PPiA), but sequence identity of these cyclophilins with cyclophilins from other organisms, like humans and yeast, is very low (17,18).

In this connection, we studied here the unfolding pathway of mitochondrial cyclophilin (CPR3) from yeast using the

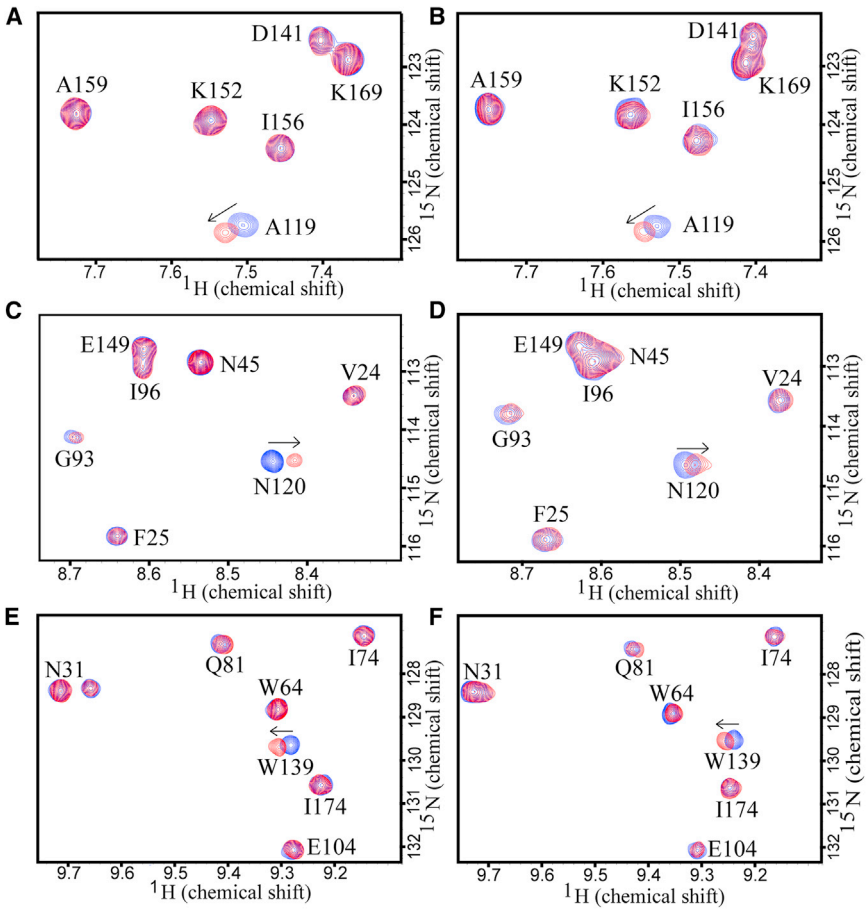

FIGURE 8 NMR spectroscopy comparison of interactions of CPR3 in 0 M and 2 M urea with peptide. (*A*, *C*, and *E*) Extracts of different regions of superimposed ^{15}N-HSQC spectra of CPR3 without urea in the absence and presence of 10 equivalents of peptide. (*B*, *D*, and *F*) Extracts of different regions of superimposed ^{15}N-HSQC spectra of CPR3 with 2 M urea in the absence and presence of 10 equivalents of the peptide. Spectra without and with the peptide are shown in blue and red, respectively. To see this figure in color, go online.

chemical denaturant urea, and the results are summarized through the schematic presentation in Fig. 9. Our investigations demonstrate that the unfolding pathway of this particular cyclophilin is specific and seems to be different from that of the other two well-studied cyclophilins, viz., LdCyp and PPiA. We observed that the denaturation curves obtained by the secondary (CD spectroscopy) and tertiary (fluorescence) structure probes were non-superimposable on each other, which suggests that the unfolding pathway of CPR3 is not a two-state reaction, N↔U. Intermediates in the unfolding pathway of CPR3 were further identified by SEC and ANS binding. SEC and comparison of the data obtained from the intrinsic fluorescence, CD spectroscopy, and ANS binding revealed the presence of two intermediates, I1 and I2, which are maximally populated at ~2 M and ~4 M urea, respectively. Thus, the unfolding pathway of CPR3 is a four-state reaction.

The I1 state is characterized by 1) native like secondary structure, 2) reduced tertiary structure, 3) strong ANS binding, 4) increased acrylamide quenching of Trp fluorescence, and 5) increased radius of gyration (molecular dimension). These observations indicate that the N-I1 transition is driven by disruption of some tertiary contacts, which results in increased exposure of Trp and other hydrophobic residues. Additionally, in NMR studies, six clusters of residues, the loop between $\alpha1$ and $\beta3$, $\beta3$ (W64–Y66, G68, and F71–R73), the loop between $\alpha1$ and $\beta3$ (W64 and Y66), $\beta4$–$\beta5$ (T88, G90, G92–K94, Y97–G98, K100–A102, D111, and A113), $\beta5$–$\beta6$ (N120, G122, N124, and N126), and the helical turn (W139–L140), show higher CSPs in the I1 state, which suggests disruption of tertiary contacts among these residues in the N-I1 transition (Fig. 5 *E*). The I2 state is characterized by 1) reduced native-like secondary and tertiary structure, and 2) higher acrylamide quenching of Trp fluorescence and higher radius of gyration, when compared to the N and I1 states. Further, the ^{15}N-HSQC spectrum displayed some peaks that seem to be from the $\alpha1$ region of the protein, suggesting retention of at least a portion of the $\alpha1$ helix. Both I1 and I2 states were found to be aggregation prone, but the aggregation kinetics profiles of these two intermediates were different. The aggregation rate of the I1 state is relatively slow compared to that of the I2 state, and secondary-structure content in the I1 aggregated state was also found to be low compared to that in the I2 aggregated state. Because of this, the size of the oligomer in the I2 state is larger than that in the I1 state, which might be due to the fact that the folded intermediate state has to first unfold to form cross-β structure.

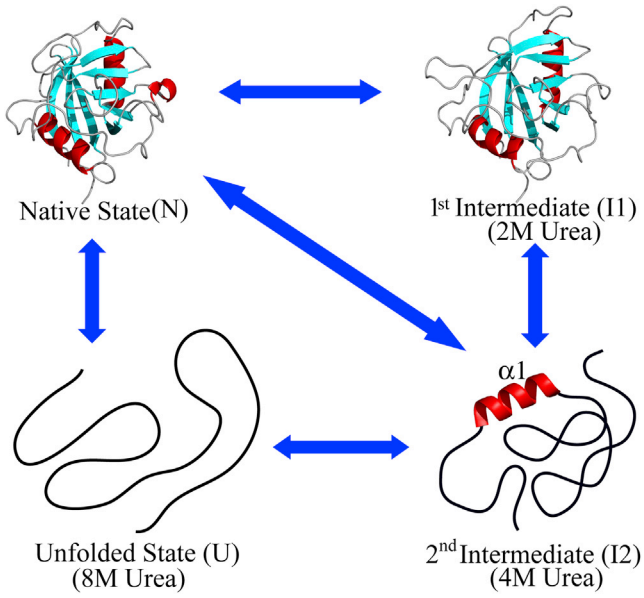

FIGURE 9 Schematic representation of urea-induced unfolding of CPR3. The structures of the native and I1 states are from residues 22–182. The structure of the I1 state was modeled by taking PDB: 2N0T (the structure of the open state) as a template. To see this figure in color, go online.

The results from ANS binding to CPR3 at different concentrations of urea for different stages of unfolding show that both the I1 and I2 states bind with ANS, though the binding affinity of the I2 state is ~3-fold weaker than that of the I1 state. These observations are suggestive of a molten-globule-like character of the I1 state; a similar type of molten-globule state was reported previously for human acidic fibroblast growth factor (hFGF-1) (47,48). The I2 state has substantial secondary structure and also shows weak ANS binding, which suggests that this state is a partly condensed state with a small solvent-accessible non-polar cluster. This inference is further confirmed by the presence of non-random coil peaks in the NMR spectrum at 4 M urea. According to the molecular theory of protein structure (proposed by (49,50) and supported by (51–53)), the secondary structure of the unfolded state fluctuates around its native-like structure, and similarly, the residual secondary and tertiary structures are native-like in the partly condensed state (49–53). In the partly condensed (I2) state of CPR3, some regions ($\alpha1$ and nearby regions) appear to exist in the native-like position in 3D space, which can be observed in the ^{15}N-HSQC spectrum having some non-random coil peaks with chemical shift similar to that in the native state.

Recently, cyclophilins were proposed to exist in two interconverting states, open and closed states, and there is a time window during which a peptide/protein interacts with the open state (16). In this study, the residues showing high CSPs in the N-I1 transition (except for K49, N53 of $\alpha1$, and K100–A102, D111, and A113 of the loop between $\beta4$ and $\beta5$) correlate well with the residues having high RMSDs in the two-state ensemble model (Fig. 5, *E* and *F*, and S4) (16). Table 1 shows a detailed comparison of the residues showing high RMSDs in the two-state ensemble and those showing high CSPs in the I1 state. These findings highlight that the I1 state of the protein may have some structural similarity to the functionally relevant "open state" of the protein.

TABLE 1 Comparison of Residues Showing High RMSD in the Two-State Ensemble and Residues Showing High CSP in the N-I1 Transition

hCypA residues showing high RMSD in the two-state ensemble	loop between α1 and β3, β3 (residues 46–55), loop between β4 and β5 (residues 62–76), loop between β5 and β6 (residues 99–103 and 108–112), loop between β6 and β7; and helical turn (residues 122–123)
CPR3 residues corresponding to the residues of hCypA, showing high RMSDs in the two-state ensemble	loop between α1 and β3, β3 (residues 64–73), loop between β4 and β5 (residues 80–94), loop between β5 and β6 (residues 117–121 and 126–130), loop between β6 and β7, and helical turn (141-142)
CPR3 residues showing high CSP in N-I1 transition	Loop between α1 and β3, β3 (residues 64–66, 68, and 71–73), loop between β4 and β5 (residues 81, 85, 88, 90–95, 100–102, 111, and 113), loop between β5 and β6 (residues 120, 122, 124, 126, and 127), loop between β6 and β7, and helical turn (residues 140–141)

Overall, the investigations of the unfolding pathway reveal that the N-I1 state transition is driven by disruption of the tertiary contacts among the loop between α1 and β3, β3, the loop between α1 and β3, β4 and β5, β5 and β6, and the helical turn of the active-site region; which results in an increase in molecular dimension and exposure of the hydrophobic surface. The I1 state has some structural similarity with the open state. The tendency of the I1 state to aggregate may have an implication inside the cell. We speculate that in certain adverse conditions the protein may get trapped in the I1 state, and also that if there is no peptide/substrate to bind, the I1 state may get converted into small oligomers with cross-β structure through structural transitions.

The results of the interaction study of CPR3 with a peptide using NMR show weak binding, as in other cyclophilins (13). The interacting residues of CPR3 were found in six main clusters in β3, β4, β5, the loops between β5 and β6 and β6 and β7, and the helical turn (Fig. 7, *A* and *C*). These regions correlate well with the earlier-reported regions for peptide interaction and catalysis in human CypA (9,16). In this study, the maximal intensity change was observed for N120, and even at low equivalents of the peptide, considerable CSP was measured. As per the earlier reports, N-H of this particular residue participates in hydrogen bonding with the preceding residue to the proline in the peptide (54). Hence, the comparison of our data with earlier reports indicates that N120 (N102 of CypA) might be one of the most important residues participating in the interaction by forming a hydrogen bond.

On comparing the unfolding pathways of CPR3, LdCyp, and PPiA, we observed that the unfolding pathway of CPR3 is different from that of the other two proteins. In LdCyp, one intermediate was reported, whereas in PPiA no intermediate was reported in the unfolding pathway (17,18). In contrast, the unfolding pathway of CPR3 occurred through stabilization of two intermediates. These two intermediates were found to be structurally different from the intermediate reported in the unfolding pathway of LdCyp. The intermediate state observed in the unfolding pathway of LdCyp has fewer native-like secondary and tertiary structures, whereas the entire secondary structure of the I1 state formed in the unfolding pathway of CPR3 is native-like, with disrupted tertiary contacts only at the active-site region. On the other hand, the I2 state has fewer native-like secondary and tertiary structures, as reported for the intermediate state in the unfolding pathway of LdCyp. However, a difference in binding of the ANS hydrophobic dye was observed. The I2 state of CPR3 shows weak binding with ANS, whereas the intermediate state of LdCyp shows strong binding with ANS. CPR3 shows high sequence identity (~65%) with human CypA, which has almost 100% sequence identity at the active site; therefore, the unfolding pathway of CypA might be expected to be similar to that of CPR3.

CONCLUSIONS

In conclusion, CPR3 has a cyclophilin-like structural fold with a β-barrel surrounded by two helices and a helical turn. The unfolding pathway of cyclophilin studied by the chemical denaturant urea is a four-state reaction (N, I1, I2, and U states) with stabilization of two intermediates. The I1 state is formed by disruption of some tertiary contacts among the five regions (the loop between α1 and β3, β3, the loops between β4 and β5 and β5 and β6, and the helical turn) well known for substrate/peptide binding. Moreover, the I1 state has some structural similarity with the open state that is reported to be involved in peptide binding. The interaction study of CPR3 with a peptide in the N and I1 states shows that residue N120 (corresponding to residue N102 of CypA) is one of the most important residues for interaction with the peptide.

SUPPORTING MATERIAL

Four figures are available at http://www.biophysj.org/biophysj/supplemental/S0006-3495(16)34324-7.

AUTHOR CONTRIBUTIONS

All experiments in the folding-unfolding study (fluorescence, CD, SEC, and NMR) were performed and analyzed by V.K.S. J.S.S. assisted in the sample preparation and recording of the different experiments. Aggregation studies were performed by N.V. and B.A. R.V.H., A.K., and V.K.S. conceived and designed the study, analyzed the results, and wrote the manuscript.

ACKNOWLEDGMENTS

We are thankful to Dipesh Kumar Trivedi for cloning the *cpr3* gene and to Priyatosh Ranjan for doing the AFM experiment at the IRCC, IIT Bombay.

We thank the Research Infrastructure Funding Committee, the Industrial Research and Consulting Centre (IRCC), the NMR facility (750 MHz), and the Bio-AFM facility at the Indian Institute of Technology (IIT) Bombay and the high-field NMR facility (800 MHz) at the Tata Institute of Fundamental Research, Mumbai. V.K.S is the recipient of research fellowships from the Department of Science and Technology-Science and Engineering Research Board, New Delhi, India. J.S.S is the recipient of research fellowships from the Ministry of Human Resource Development, IIT Bombay, Mumbai, India. A.K. is thankful to the IRCC, IIT Bombay for a seed grant. B.A. gratefully acknowledges the University Grants Commission-Faculty Recharge Program (UGC-FRP) of the Government of India for awarding him a UGC Assistant Professor position.

REFERENCES

1. Wang, P., and J. Heitman. 2005. The cyclophilins. *Genome Biol.* 6:226.
2. Laupacis, A., P. A. Keown, …, C. R. Stiller. 1982. Cyclosporin A: a powerful immunosuppressant. *Can. Med. Assoc. J.* 126:1041–1046.
3. Kallen, J., C. Spitzfaden, …, M. D. Walkinshaw. 1991. Structure of human cyclophilin and its binding site for cyclosporin A determined by x-ray crystallography and NMR spectroscopy. *Nature.* 353:276–279.
4. Nigro, P., G. Pompilio, and M. C. Capogrossi. 2013. Cyclophilin A: a key player for human disease. *Cell Death Dis.* 4:e888.
5. Howard, B. R., F. F. Vajdos, …, C. P. Hill. 2003. Structural insights into the catalytic mechanism of cyclophilin A. *Nat. Struct. Biol.* 10:475–481.
6. Ottiger, M., O. Zerbe, …, K. Wüthrich. 1997. The NMR solution conformation of unligated human cyclophilin A. *J. Mol. Biol.* 272:64–81.
7. Spitzfaden, C., W. Braun, …, K. Wüthrich. 1994. Determination of the NMR solution structure of the cyclophilin A-cyclosporin A complex. *J. Biomol. NMR.* 4:463–482.
8. Saleh, T., W. Jankowski, …, C. G. Kalodimos. 2016. Cyclophilin A promotes cell migration via the Abl-Crk signaling pathway. *Nat. Chem. Biol.* 12:117–123.
9. Eisenmesser, E. Z., D. A. Bosco, …, D. Kern. 2002. Enzyme dynamics during catalysis. *Science.* 295:1520–1523.
10. Kofron, J. L., P. Kuzmic, …, D. H. Rich. 1991. Determination of kinetic constants for peptidyl prolyl *cis-trans* isomerases by an improved spectrophotometric assay. *Biochemistry.* 30:6127–6134.
11. Zhao, Y., and H. Ke. 1996. Mechanistic implication of crystal structures of the cyclophilin-dipeptide complexes. *Biochemistry.* 35:7362–7368.
12. Zhao, Y., Y. Chen, …, H. Ke. 1997. Cyclophilin A complexed with a fragment of HIV-1 gag protein: insights into HIV-1 infectious activity. *Structure.* 5:139–146.
13. Camilloni, C., A. B. Sahakyan, …, M. Vendruscolo. 2014. Cyclophilin A catalyzes proline isomerization by an electrostatic handle mechanism. *Proc. Natl. Acad. Sci. USA.* 111:10203–10208.
14. Vögeli, B., S. Kazemi, …, R. Riek. 2012. Spatial elucidation of motion in proteins by ensemble-based structure calculation using exact NOEs. *Nat. Struct. Mol. Biol.* 19:1053–1057.
15. Vögeli, B. 2014. The nuclear Overhauser effect from a quantitative perspective. *Prog. Nucl. Magn. Reson. Spectrosc.* 78:1–46.
16. Chi, C. N., B. Vögeli, …, R. Riek. 2015. A structural ensemble for the enzyme cyclophilin reveals an orchestrated mode of action at atomic resolution. *Angew. Chem. Int. Ed. Engl.* 54:11657–11661.
17. Roy, S., S. Basu, …, D. Dasgupta. 2014. Equilibrium unfolding of cyclophilin from *Leishmania donovani*: characterization of intermediate states. *Int. J. Biol. Macromol.* 69:353–360.
18. Mitra, D., S. Mukherjee, and A. K. Das. 2006. Cyclosporin A binding to *Mycobacterium tuberculosis* peptidyl-prolyl *cis-trans* isomerase A—investigation by CD, FTIR and fluorescence spectroscopy. *FEBS Lett.* 580:6846–6860.
19. Shukla, V. K., J. S. Singh, …, A. Kumar. 2016. NMR assignments of mitochondrial cyclophilin Cpr3 from *Saccharomyces cerevisiae*. *Biomol. NMR Assign.* 10:203–206.
20. Wishart, D. S., D. Arndt, …, G. Lin. 2008. CS23D: a web server for rapid protein structure generation using NMR chemical shifts and sequence data. *Nucl. Acids Res.* 36:W496–W502.
21. Eftink, M. R., and C. A. Ghiron. 1981. Fluorescence quenching studies with proteins. *Anal. Biochem.* 114:199–227.
22. Fersht, A. R. 1999. Structure and Mechanism in Protein Science. W.H. Freeman, London, United Kingdom.
23. Sanz, J. M., and A. R. Fersht. 1993. Rationally designing the accumulation of a folding intermediate of barnase by protein engineering. *Biochemistry.* 32:13584–13592.
24. Uversky, V. N., and O. B. Ptitsyn. 1994. "Partly folded" state, a new equilibrium state of protein molecules: four-state guanidinium chloride-induced unfolding of β-lactamase at low temperature. *Biochemistry.* 33:2782–2791.
25. Uversky, V. N., and O. B. Ptitsyn. 1996. Further evidence on the equilibrium "pre-molten globule state": four-state guanidinium chloride-induced unfolding of carbonic anhydrase B at low temperature. *J. Mol. Biol.* 255:215–228.
26. Wishart, D. S., B. D. Sykes, and F. M. Richards. 1991. Relationship between nuclear magnetic resonance chemical shift and protein secondary structure. *J. Mol. Biol.* 222:311–333.
27. Shukla, V. K., A. Kabra, …, A. Arora. 2015. Solution structures and dynamics of ADF/cofilins UNC-60A and UNC-60B from *Caenorhabditis elegans*. *Biochem. J.* 465:63–78.
28. Borana, M. S., P. Mishra, …, B. Ahmad. 2014. Curcumin and kaempferol prevent lysozyme fibril formation by modulating aggregation kinetic parameters. *Biochim. Biophys. Acta.* 1844:670–680.
29. Shen, Y., F. Delaglio, …, A. Bax. 2009. TALOS+: a hybrid method for predicting protein backbone torsion angles from NMR chemical shifts. *J. Biomol. NMR.* 44:213–223.
30. Lakowicz, J. R. 1983. Principles of Fluorescence Spectroscopy. Plenum Press, New York.
31. Prajapati, S., V. Bhakuni, …, S. K. Jain. 1998. Alkaline unfolding and salt-induced folding of bovine liver catalase at high pH. *Eur. J. Biochem.* 255:178–184.
32. Ahmad, A., M. S. Akhtar, and V. Bhakuni. 2001. Monovalent cation-induced conformational change in glucose oxidase leading to stabilization of the enzyme. *Biochemistry.* 40:1945–1955.
33. Tripathi, T., B. K. Na, …, V. Bhakuni. 2009. Structural, functional and unfolding characteristics of glutathione S-transferase of *Plasmodium vivax*. *Arch. Biochem. Biophys.* 487:115–122.
34. Ahmad, B., M. Z. Ahmed, …, R. H. Khan. 2005. Guanidine hydrochloride denaturation of human serum albumin originates by local unfolding of some stable loops in domain III. *Biochim. Biophys. Acta.* 1750:93–102.
35. Ahmad, B., T. A. Shamim, …, R. H. Khan. 2007. Identification and characterization of functional intermediates of stem bromelain during urea and guanidine hydrochloride unfolding. *J. Biochem.* 141:251–259.
36. Hargrove, M. S., S. Krzywda, …, J. S. Olson. 1994. Stability of myoglobin: a model for the folding of heme proteins. *Biochemistry.* 33:11767–11775.
37. Uversky, V. N., G. V. Semisotnov, …, O. B. Ptitsyn. 1992. "All-or-none" mechanism of the molten globule unfolding. *FEBS Lett.* 314:89–92.
38. Uversky, V. N. 1993. Use of fast protein size-exclusion liquid chromatography to study the unfolding of proteins which denature through the molten globule. *Biochemistry.* 32:13288–13298.
39. Xue, W. F., S. W. Homans, and S. E. Radford. 2008. Systematic analysis of nucleation-dependent polymerization reveals new insights into

the mechanism of amyloid self-assembly. *Proc. Natl. Acad. Sci. USA.* 105:8926–8931.

40. Muthu, S. A., N. Mothi, …, B. Ahmad. 2016. Physical basis for the ofloxacin-induced acceleration of lysozyme aggregation and polymorphism in amyloid fibrils. *Arch. Biochem. Biophys.* 592:10–19.
41. Ahmad, B., J. Winkelmann, …, F. Chiti. 2010. Searching for conditions to form stable protein oligomers with amyloid-like characteristics: the unexplored basic pH. *Biochim. Biophys. Acta.* 1804:223–234.
42. Mastrangelo, I. A., M. Ahmed, …, S. O. Smith. 2006. High-resolution atomic force microscopy of soluble Aβ42 oligomers. *J. Mol. Biol.* 358:106–119.
43. Ahmad, B., I. Vigliotta, …, F. Chiti. 2011. The induction of α-helical structure in partially unfolded HypF-N does not affect its aggregation propensity. *Protein Eng. Des. Sel.* 24:553–563.
44. Voropai, E. S., M. P. Samtsov, …, V. N. Uverskii. 2003. Spectral properties of thioflavin T and its complexes with amyloid fibrils. *J. Appl. Spectrosc.* 70:868–874.
45. Vaynberg, J., and J. Qin. 2006. Weak protein-protein interactions as probed by NMR spectroscopy. *Trends Biotechnol.* 24:22–27.
46. Williamson, M. P. 2013. Using chemical shift perturbation to characterise ligand binding. *Prog. Nucl. Magn. Reson. Spectrosc.* 73:1–16.
47. Semisotnov, G. V., N. A. Rodionova, …, R. I. Gilmanshin. 1991. Study of the "molten globule" intermediate state in protein folding by a hydrophobic fluorescent probe. *Biopolymers.* 31:119–128.
48. Samuel, D., T. K. Kumar, …, C. Yu. 2000. Identification and characterization of an equilibrium intermediate in the unfolding pathway of an all β-barrel protein. *J. Biol. Chem.* 275:34968–34975.
49. Ptitsyn, O. B., and A. V. Finkelstein. 1980. Similarities of protein topologies: evolutionary divergence, functional convergence or principles of folding? *Q. Rev. Biophys.* 13:339–386.
50. Ptitsyn, O. B., and A. V. Finkelstein. 1983. Theory of protein secondary structure and algorithm of its prediction. *Biopolymers.* 22:15–25.
51. Dyson, H. J., and P. E. Wright. 1993. Peptide conformation and protein folding. *Curr. Opin. Struct. Biol.* 3:60–65.
52. Dyson, H. J., G. Merutka, …, P. E. Wright. 1992. Folding of peptide fragments comprising the complete sequence of proteins. Models for initiation of protein folding. I. Myohemerythrin. *J. Mol. Biol.* 226:795–817.
53. Waltho, J. P., V. A. Feher, …, P. E. Wright. 1993. Peptide models of protein folding initiation sites. 1. Secondary structure formation by peptides corresponding to the G- and H-helices of myoglobin. *Biochemistry.* 32:6337–6347.
54. Hur, S., and T. C. Bruice. 2002. The mechanism of *cis-trans* isomerization of prolyl peptides by cyclophilin. *J. Am. Chem. Soc.* 124:7303–7313.